Research Article | Vol. 28, No. 15 / 20 July 2020 / Optics Express 21348
Optics EXPRESS

Impact of spectral filtering on pulse breaking-up and noise-like pulse generation in all-normal dispersion fiber lasers

RUNQIN XU,[1] FANJIANG XU,[2] YANRONG SONG,[3] LEI DUAN,[2,*] YUNBO SONG,[2] SHUDAN TAN,[2] AND ZHAOHUI LIU[2]

[1]Institute of Automation, Chinese Academy of Sciences, Beijing 100190, China
[2]Institute of Software, Chinese Academy of Sciences, Beijing 100190, China
[3]College of Applied Sciences, Beijing University of Technology, Beijing 100124, China
*duanlei@iscas.ac.cn

Abstract: Based on mathematic simulations, the impact of spectral filtering on pulse breaking up and noise-like pulse generation in all-normal-dispersion fiber lasers are investigated. Three types of spectrum filters are employed in the simulations, which have a Gaussian-shaped profile, super-Gaussian-shaped profile, and sinusoidal-shaped profile, respectively. With the Gaussian-shaped filter, the pulse breaking-up process is discussed. The super-Gaussian-shaped filter and the sinusoidal-shaped filter have two different formation mechanisms for noise-like pulses and are revealed. In addition, with the sinusoidal-shaped filter, dissipative solitons of different central wavelengths are achieved.

© 2020 Optical Society of America under the terms of the OSA Open Access Publishing Agreement

1. Introduction

Passively mode-locked fiber lasers have been extensively investigated and greatly developed in the past two decades for their compactness, efficiency and high beam quality. They are now widely applied in many areas such as communication, spectroscopy, supercontinuum generation, frequency comb generation, optical sensing, etc. In order to achieve mode-locking pulses with higher single pulse energy, different types of pulse regimes have been explored, which mainly include conventional solitons [1], stretched pulses [2], similaritons [3], dissipative solitons (DS) [4], dissipative soliton resonance (DSR) [5] and noise-like pulses (NLP) [6,7]. For conventional soliton pulses and stretched pulses, the pulse energies are confined due to the soliton inherency. In similariton lasers, a dispersion delay line, such as a pair of gratings, is usually needed to make the pulses satisfy the condition of self-reproduction. DSR and NLP are generally considered as wave-breaking free. At the expense of pulse duration expansion, their pulse energies can be improved to an appreciable level. However, both of them can hardly be compressed. By now, dissipative soliton lasers play a dominant role in achieving high energy ultrashort pulses.

Dissipative solitons with single pulse energies more than 10 nJ could be obtained in all-normal dispersion (ANDi) fiber lasers via various mode-locking techniques such as nonlinear polarization (NPR) [8], semiconductor saturable absorber mirror (SESAM) [9] and nonlinear loop mirrors (NOLM) [10,11]. However, under strong pump strength, the DS may either break up or evolve into NLP, thus the achievable single pulse energies for DS are limited. In order to obtain DS with higher single pulse energies, the mechanisms leading to pulse breaking-up and NLP need to be circumvented. Based on theoretical investigations, some previous researches have pointed out that spectral filtering is closely related to the formations of multi-pulse regime and the noise-like pulse regime [12–16]. In these corresponding researches, the spectrum filters were usually assumed to have transmission curves of a Gaussian profile. The impact of the shape of the filter transmission curve were not especially tended. However, in the experiments, several types of spectrum filters with different transmission curves are often used. For example, except for the Gaussian-shaped

#391186 https://doi.org/10.1364/OE.391186
Journal © 2020 Received 24 Feb 2020; revised 9 Apr 2020; accepted 28 Apr 2020; published 6 Jul 2020

Optics EXPRESS

filter, bandpass filters made by grating pair and knife edges [17] may have super-Gaussian-shaped profiles whereas the birefringent filters [18] generally have sinusoidal-shaped profiles.

In this article, the impact of the shape of the filter profiles on the pulse breaking-up and noise-like pulse generation in ANDi fiber lasers are theoretically researched. Three types of profiles are employed in the simulations: Gaussian-shaped, super-Gaussian-shaped, and sinusoidal-shaped, respectively. The research may provide deeper understandings of the pulse dynamics in the ANDi fiber lasers and might also offer new perspectives to view how to achieve DS with high single pulse energies.

2. Theoretical model

A typical Yb-doped mode-locked ANDi fiber laser is considered as schematically shown in Fig. 1. The simulated system contains one segment of Yb-doped single mode fiber, three segments of undoped single mode fiber, a saturable absorber (SA), an output coupler (OC) and a spectrum filter (SF).

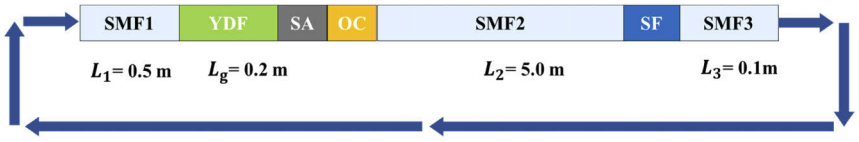

Fig. 1. Schematic of the simulated mode-locked ANDi Yb-doped fiber laser. SMF: single mode fiber; YDF: Yb-doped fiber; SA: saturable absorber; OC: output coupler; SF: spectrum filter. L_1, L_2, L_3 and L_g are the lengths of different fiber segments.

To model the pulse evolution in fibers, the complex nonlinear Ginzburg-Landau equation is used:

$$\frac{\partial A}{\partial z} = -\frac{\mathrm{i}}{2}\beta_2\frac{\partial^2 A}{\partial t^2} + \mathrm{i}\gamma|A|^2A + \frac{g}{2}A + \frac{g}{2\Omega_g^2}\frac{\partial^2 A}{\partial t^2} \tag{1}$$

where A is the electric envelope of the pulse; β_2 and γ are the group velocity dispersion (GVD) coefficient and nonlinear coefficient of the fiber, which are set to 18×10^{-3} ps^2/m and 2.6×10^{-3} W^{-1}m^{-1} for both the active and passive fiber; g represents the saturable gain of the fiber. The last term of Eq. (1) is related to the gain bandwidth limitation. The gain curve has a parabolic shape with a maximum value of g. In Ref [19]., Ω_g is treated as the gain bandwidth while the 3 dB (FWHM) bandwidth is $\sqrt{2}\Omega_g$. In the simulation, Ω_g is set to 20 nm. The saturable gain g could be expressed as

$$g = g_0\exp\left(-\frac{E}{E_{\mathrm{sat}}}\right) \tag{2}$$

Here, g_0 is the small signal gain coefficient; E_{sat} is the gain saturation energy; E is the intracavity pulse energy. For the active fiber, g_0 is 8 m^{-1} while for the passive fibers g_0 is set to 0 m^{-1}. The gain saturation energy is variable so that the pump strength can be adjusted.

SAs can be classified as artificial SAs and physical SAs. An artificial SA refers to a system composed of several devices that are able to provide a saturable absorption effect and is usually employed for studying mode-locked fiber lasers utilizing NPR or NOLM techniques. A physical SA is usually a single device or a kind of material, such as SESAM, graphene, carbon nanotube and so on. In our simulation, the physical SA is used, whose transmission function can be

Optics EXPRESS

expressed as

$$T_{\mathrm{SA}} = 1 - \left[\alpha_{\mathrm{ns}} + \alpha_0 / \left(1 + \frac{|A|^2}{P_{\mathrm{SA}}}\right)\right] \tag{3}$$

where α_{ns} and α_0 are the non-saturated loss and modulation depth; P_{SA} is the saturation power. The values of the three parameters are set to 5 %, 40 %, and 100 W, respectively. The output ratio of the OC is set to 20 %.

SFs with three different types of transmission curves are employed, which are Gaussian-shaped, super-Gaussian-shaped and sinusoidal-shaped curves, respectively. The Gaussian-shaped SF is modeled as

$$T = T_{\max} \exp\left[-\frac{(\lambda - \lambda_0)^2}{2\,(\Delta\lambda/2.355)^2}\right] \tag{4}$$

in which $T_{\max}$ is the maximum transmissivity of the SF. $\Delta\lambda$ is the FWHM bandwidth. λ_0 is the central wavelength of the filter. The model of the super-Gaussian-shaped SF can be simply revised from Eq. (4), expressed as

$$T = T_{\max} \exp\left[-\frac{(\lambda - \lambda_0)^{2m}}{2\,(\Delta\lambda/2.355)^{2m}}\right], \quad m>1 \tag{5}$$

In our simulation, m is set to 25. Correspondingly, its FWHM bandwidth is about 0.855 $\Delta\lambda$. Because of the sharp edges, 0.855 $\Delta\lambda$ could also be considered as the distance between the leading edge and the trailing edge of the transmission curve. The mathematic expression of the sinusoidal-shaped SF could be written as

$$T = \frac{T_{\max} - T_{\min}}{2} \cos\left[\frac{\pi}{\Delta\lambda/2.355}(\lambda - \lambda_0) + \phi\right] + \frac{T_{\max} + T_{\min}}{2} \tag{6}$$

$T_{\min}$ is the minimum transmissivity of the sinusoidal-shaped filter; ϕ is a variable phase used for shifting the transmission curve. Since the transmission curve is a periodic function, it actually has no FWHM bandwidth. Here, we can define the half period as the FWHM bandwidth, which is $\Delta\lambda/2.355$. Figure 2 is a brief illustration of the transmission curves. In the simulation, $T_{\max}$ and λ_0 are set to 99% and 1038 nm for all the three types of SFs.

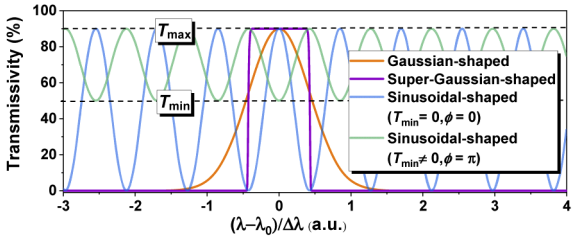

Fig. 2. An illustration of the transmission curves of the filters.

To simulate mode-locking, the pulse tracking technique is adopted [20]. Briefly, the simulation starts with an injected arbitrary weak pulse, which circulates in the ring cavity till a steady state is established. Here, the arbitrary weak pulse is given as a chirp-free sech-shaped pulse with 10 ps pulse duration (3 dB) and 5×10^{-6} pJ single pulse energy.

3. Simulation results and discussions

In the simulation, it is discovered that when the pump strength is improved and/or the filter bandwidth decreases: (1) for the Gaussian-shaped filter, DS tend to split into multiple pulses; (2)

Optics EXPRESS

for the super-Gaussian-shaped filter, NLP are more favored; (3) for the sinusoidal-shaped filter, multiple DS with different central wavelengths or NLP may occur. The simulation results will be detailedly discussed in next subsections.

3.1. DS in single-pulse regime with different filters

To have a better understanding of the formations of the multi-pulse regime and the noise-like pulse regime, it is necessary to investigate how DS vary with pump strength and filter bandwidth within the single-pulse regime. Keeping the fiber laser operating in the single-pulse state, we measured the pulse energy, pulse duration, peak power and spectral width of the output pulses from the OC under different filter bandwidths and pump strengths. Figures 3(a) and 3(b) exhibit the simulation results corresponding to the Gaussian-shaped filter and the super-Gaussian-shaped filter, respectively (the simulation results of the sinusoidal-shaped filter are similar to the Gaussian-shaped filter, therefore is not exhibited here).

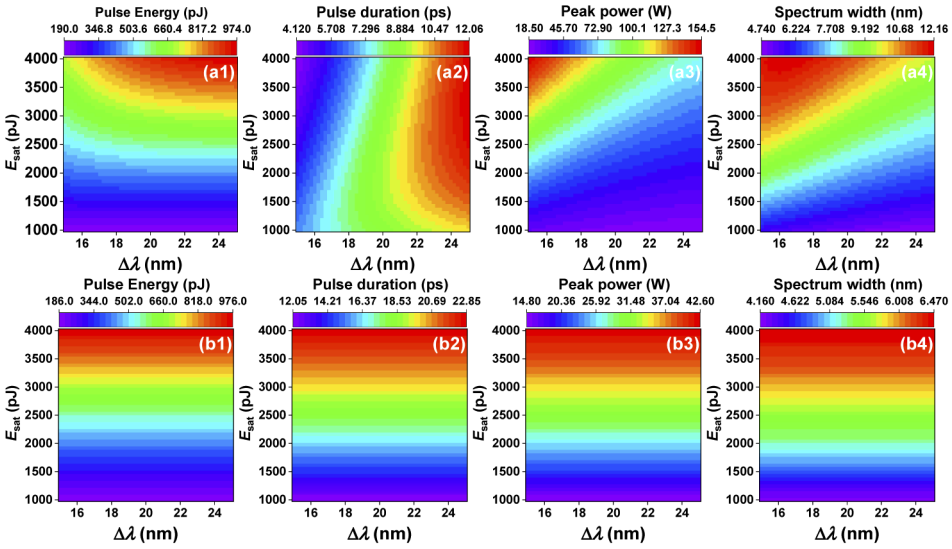

Fig. 3. Single pulse energy, peak power, pulse duration and spectrum width of the output pulses from the OC under different filter bandwidths and pump strengths for the Gaussian-shaped and super-Gaussian-shaped filter. (a) Gaussian-shaped filter; (b) super-Gaussian-shaped filter.

Basically, the impact of the SF on DS mode-locking includes three aspects: firstly, the SF modulates the pulse spectrum; secondly, the SF introduces a spectrum-related loss to the pulse; lastly, due to the approximately monotonous positive-chirp of DS [4], the SF could also narrow the pulse envelope when filtering the spectrum.

For the Gaussian-shaped filter, when $\Delta\lambda$ is increased, the loss induced by the SF decreases, hence the pulse energy increases (see Fig. 3(a1)). Meanwhile, the pulse-narrowing-ability of the SF weakens, therefore the pulse duration goes up (see Fig. 3(a2)), which then results in peak power declining (see Fig. 3(a3)). Since lower peak power causes less nonlinear phase accumulation, the spectrum width also declines (see Fig. 3(a4)). When the pump strength changes, from a cursory perspective, all the four parameters show positive correlations with the pump strength. As for the distortion in Fig. 3(a2) that in some areas the pulse duration increases with the improvement of the pump strength, it could be attributed to the stronger pulse broadening effect (caused by dispersion) resulted from the wider spectrum.

Optics EXPRESS

For the super-Gaussian-shaped filter, because its transmission curve has a nearly flat top, the effect of the SF can be quite slight if the spectrum width is narrower than about 0.855 $\Delta\lambda$. Therefore, in Fig. 3(b) all the four parameters barely vary versus $\Delta\lambda$. But when the pump strength is improved, all these four parameters increase. Though the super-Gaussian-shaped filter seems insignificant here, it could actually prevent the spectrum and the pulse envelope from infinitely growing wide, which is essential for stabilizing the mode-locking the ANDi fiber laser.

3.2. DS breaking up with Gaussian-shaped filter

Because of the nearly monotonous chirp of DS, the Gaussian-shaped filter could impose an attenuation on the pulse, which is related to the pulse spectrum width. Hence, the final achievable single pulse energy of a dissipative soliton is limited by the filter. If the filter bandwidth is too narrow and/or the pump strength is too strong, making the pulse energy drop far below the gain saturation energy, a strong extra gain will occur. The strong extra gain can amplify some small signals such as background noises into sub-pulses, making the dissipative soliton break up. In short, the two key points for the dissipative soliton breaking-up are strong extra gain and small signals to be amplified.

Figure 4 describes a dissipative soliton breaking-up process (see Visualization 1). E_{sat} is fixed at 2500 pJ; $\Delta\lambda$ is firstly set to 15 nm to obtain a stable dissipative soliton mode-locking state, then changed to 10 nm to achieve the pulse breaking-up. During the pulse evolution, if the pulse does not match with the laser cavity, the pulse will keep shaping itself to meet the requirement of self-reproduction. In this process, the pulse will keep emitting dispersive waves (see Figs. 4(c) and 4(e)) into the background. Here, the dispersive waves are mainly generated by spectrum filtering. These dispersive waves will may fade away or be amplified by the extra gain. Once being amplified to a considerable level, pulse breaking-up happens (see Figs. 4(f) and 4(g)). After the pulse breaking up, the total intracavity pulse energy will slightly increase, then the extra gain decreases and may not support amplifying small signals anymore, which stops further pulse breaking-up.

It is worth noting that in Fig. 4 the main pulse disappears at last. This is because the main pulse has larger chirp than the sub-pulses due to more nonlinear phase accumulation in previous iterations (see Fig. 4(f)). Thus, the main pulse experiences more attenuation at the SF, which makes it tend to lose in the gain competition with the newly generated sub-pulses, leading to its degeneration. However, if the pump strength is strong enough, the main pulse could be amplified again, which is actually the situation that a dissipative soliton breaks up into three pulses. Figure 5 (see Visualization 2) shows the degeneration and the regeneration of the main pulse. The simulation setting for Fig. 5 is the same as Fig. 4 except that E_{sat} is improved to 4000 pJ. To conveniently compare the spectrum width, the Wigner distribution is utilized here.

3.3. NLP generated with super-Gaussian-shaped filter

From Fig. 3(b), it could be found out that when the super-Gaussian-shaped filter is used, as long as the pulse spectrum width is narrower than 0.855 $\Delta\lambda$, the intracavity pulse energy will remain either close to or higher than the gain saturation energy, which means that there is no much extra gain in the cavity. Without strong extra gain, the multi-pulse state can hardly occur. On the other hand, if the pump strength is strong enough and/or the filter bandwidth is small enough, the spectrum width will exceed 0.855 $\Delta\lambda$, extending out the edges of the SF transmission curves. Under this circumstance, the fiber laser tends to operate in the noise-like pulse regime. A noise-like pulse is generally considered as a wave packet that contains a lot of random fine structures or sub-pulses within it. Its intensity autocorrelation (IAC) trace is two-scaled, consisting of a pedestal and a spike. The widths of the pedestal and the spike indicate the width of the wave packet and the average width of the sub-pulses inside the wave packet,

Optics EXPRESS

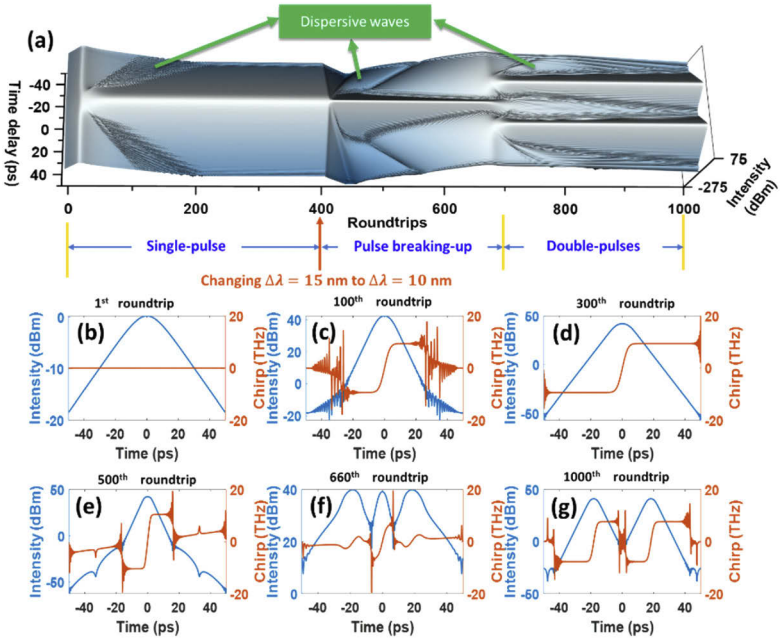

Fig. 4. A dissipative soliton breaks up into two pulses via changing the filter bandwidth from 15 nm to 10 nm with a gain saturation energy of 2500 pJ. (a) Pulse evolution in log scale; (b-g) pulse envelops in log scale and corresponding chirps at different roundtrips. (See Visualization 1)

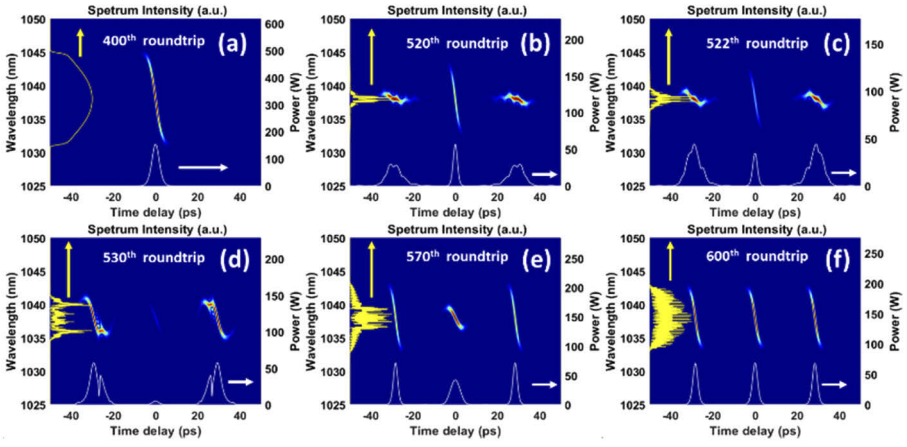

Fig. 5. Wigner distributions with pulse envelopes and spectra at different roundtrips. The main pulse degenerates firstly, then it is amplified again and finally leads to the three-pulse state. (See **Visualization 2**)

Optics EXPRESS

respectively; the ratio of the spike to the pedestal is related to the density of sub-pulse that a larger ratio usually means a smaller sub-pulse density [21].

Setting E_{sat} to 4000 pJ and $\Delta\lambda$ to 6 nm, NLP could be generated as shown in Fig. 6 (see Visualization 3). The pulse envelope, pulse chirp, and spectrum are all chaos-like (see Figs. 6(c) and 6(d)). The IAC trace of the pulse is two-scaled (see Fig. 6(e)), composed of a wide pedestal and a narrow coherent spike, which exhibits the typical shape of the IAC trace of NLP.

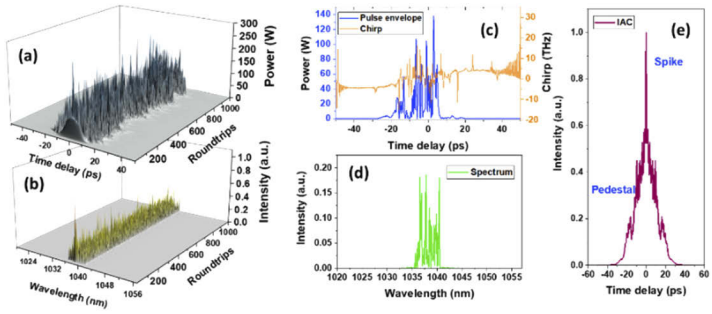

Fig. 6. NLP generated with the super-Gaussian-shaped filter. (a) and (b) 3D colormap surfaces and corresponding projections of the evolutions of the pulse envelope and spectrum; (c) pulse envelope with chirp; (d)spectrum; (e) IAC trace of the output pulse at the 1000th simulation roundtrip. (See Visualization 3)

To figure out how the SF affects the noise-like pulse generation, the pulses at the 33th–36th roundtrips where the noise-like pulse starts to form are sliced out to observe the pulse envelopes and spectra before and after the SF. The results are depicted in Fig. 7. The modulation of the SF on the pulse envelope could be calculated by convoluting the pulse envelope with the inverse Fourier transformation (IFT) of the filter transmission curve. Considering that the filter transmission curve resembles a gate-function, its IFT should be similar to a sinc-function which consists of a main peak and many sidelobes. Because of these sidelobes, in Fig. 7(a) it could be determined that when the pulse passes through the SF, some fluctuations are introduced to the pulse envelope. The fluctuations are then enhanced over and over every time the pulse passing through the SF. With more and more fluctuations introduced, the pulse envelope eventually becomes chaotic-like. We believe this is the main reason why the noise-like pulse is generated. On the other hand, because of the self-phase modulation effect, there are fluctuations generated in the pulse spectrum (see Fig. 7(b)), too. However, having a flat top in the transmission curve, the SF can hardly suppress these spectral fluctuations, which eventually leads to a chaotic-like spectrum. This may also contribute to noise-like pulse formation.

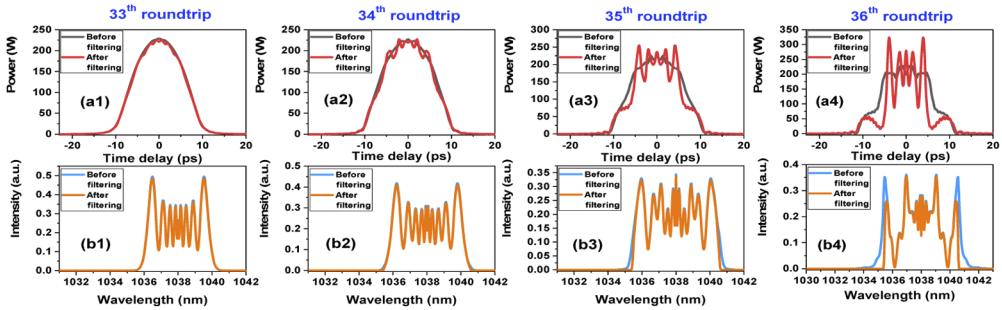

Fig. 7. Pulse envelopes and spectra before and after the modulation of the super-Gaussian-shaped filter at the 33th–36th roundtrips. (a) Pulse envelopes; (b) pulse spectra.

Optics EXPRESS

Furthermore, the influences of the variation of the super-Gaussian-shaped filter bandwidth on the noise-like pulse state are investigated. Figure 8 depicts the pulse envelopes, spectra and IAC traces of the output pulses at 500th roundtrips, corresponding to $\Delta\lambda$ = 4, 6, 8, 10 and 12 nm, respectively. Figure 8(b) clearly shows that the spectrum range grows wider with the increase of $\Delta\lambda$. Meanwhile, since super-Gaussian-shaped filter with larger bandwidth introduces fewer fluctuations on the pulse envelope, the pulse gradually turns into non-NLP as is described in Fig. 8(a), which then results in the spike of the IAC trace becomes more and more inconspicuous as exhibited in Fig. 8(c). For $\Delta\lambda$ of 8 and 10 nm, their pulse envelopes shown in Figs. 8(a2)–8(a3) are obviously less noise-like than in Figs. 8(a4)–8(a6) with $\Delta\lambda$ of 2, 4 and 6 nm; for $\Delta\lambda$ of 12 nm, the generated pulse is a dissipative soliton rather than a noise-like pulse. On the other hand, the variation of the filter bandwidth could also affect the duration of the sub-pulses within the noise-like pulse. According to our previous research [17], the wider the noise-like pulse spectrum is, the narrower the sub-pulses within the noise-like pulse can be. This trend can be seen in Figs. 8(a4)–8(a6) as well, which is consistent with the variation of the spike width in Fig. 8(c4)–8(c6), in which the spike widths for $\Delta\lambda$ of 2, 4 and 6 nm are about 1520 fs, 820 fs and 680 fs, respectively.

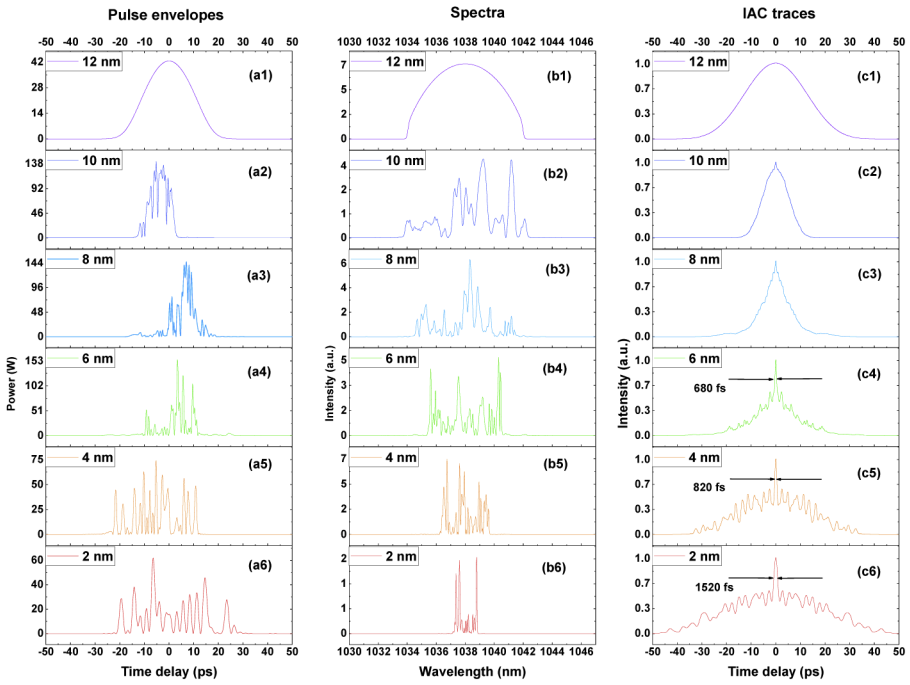

Fig. 8. Pulse envelopes, spectra and IAC traces of the output pulses at 500th roundtrips corresponding to $\Delta\lambda$ of 4,6,8,10 and 12 nm, respectively. (a) Pulse envelopes; (b) pulse spectra; (c) IAC traces.

3.4. *Dual-wavelength DS and NLP generated with sinusoidal-shaped filter*

Due to more adjustable parameters, the mode-locking results with the sinusoidal-shaped filter are versatile. In this subsection, we only focus on the dual-wavelength DS and NLP. The sinusoidal transmission curve has multiple peaks, which make it possible for DS with different central wavelengths to survive in the cavity. For example, setting $\Delta\lambda = 20$ nm, $E_{sat} = 2000$ pJ, $T_{min} = 0$ and $\phi = \pi$, we could obtain two DS with different central wavelengths. Figure 9 shows their

Optics EXPRESS

Wigner distributions together with the pulse envelopes and spectra. Since the two DS have different central wavelengths, their group velocities also differ from each other, which brings about pulse collision. It seems that the pulse collision barely affects the mode-locking stability but will generate interference fringes in the time domain which can be found in Fig. 9(c). For Fig. 9 (see Visualization 4), it should be noticed that when the pulse steps out the time window from one side, it will enter the time window simultaneously from the other side, because there is no absorber layer in the simulation. We believe this is reasonable, which just matches the assumption of the ring cavity except that the time window is much narrower than the actual cavity roundtrip time.

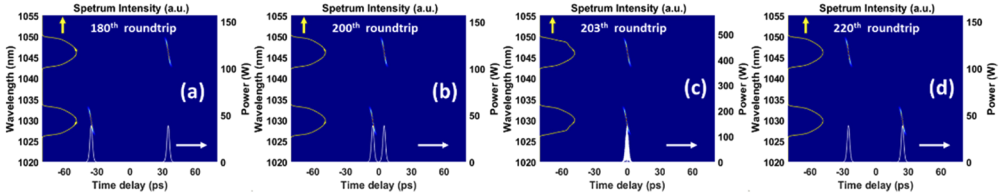

Fig. 9. Wigner distributions, pulse envelopes and spectra of the dual-wavelengths DS at different roundtrips. (See Visualization 4)

If $\Delta\lambda$ is decreased and E_{sat}, T_{min} are increased, dual-wavelength DS can no longer be achieved while the noise-like pulse is generated instead. For instance, setting $\Delta\lambda = 5$ nm, $E_{sat} = 8000$ pJ, $T_{min} = 0.9$ and $\phi = \pi$, noise-like pulse mode-locking is obtained as is shown in Fig. 10. In order to figure out how the noise-like pulse is generated, the pulses at the 50^{th} ~120^{th} simulation roundtrips are sliced out and their Wigner distributions are calculated, which are depicted in Fig. 11 (see Visualization 5). One can notice that in Figs. 11(a)–11(d), the pulse exhibits several obvious peaks with different central wavelengths, which should be caused by the multiple peaks in the filter profile as well as the formation of the dual-wavelength DS. Due to different group velocities, these peaks gradually walk off from the center of the pulse. Meanwhile, new peaks are generated at the center. With the increase of the pulse energy, the peaks become wider and higher. Thereafter, interferences between these peaks happen, which bring about interference fringes in the time domain (see Fig. 11(h)). These interference fringes should be the origin of the noise-like pulse. Moreover, the variation of spectrum component near the pulse center (see Figs. 11(b)–11(g)) indicates the energy exchanges between these peaks.

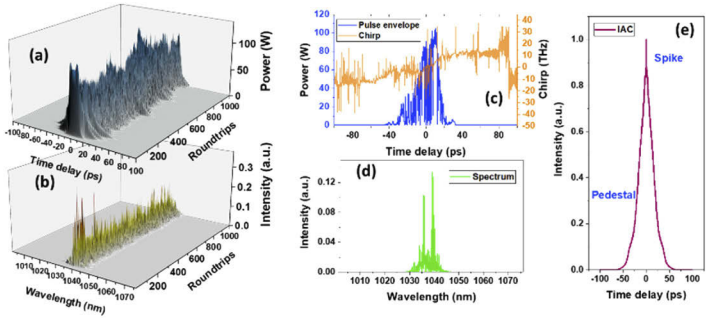

Fig. 10. NLP generated with a sinusoidal-shaped filter. (a) and (b) 3D colormap surfaces and corresponding projections of the evolutions of the pulse envelope and spectrum; (c) pulse envelope with chirp; (d)spectrum; (e) IAC trace of the output pulse at the 1000^{th} roundtrip. (See Visualization 5)

Optics EXPRESS

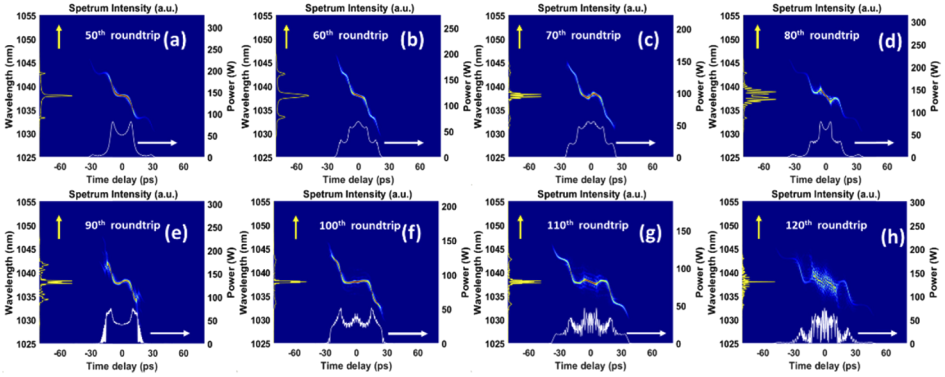

Fig. 11. Wigner distributions with pulse envelopes and spectra of the NLP at 50^{th} ~120^{th} roundtrips. (Also see Visualization 5)

It could be found that the continuous interference between the multiple peaks plays a dominant role in the generation of NLP. Further simulations indicate that there are two main requirements for the sinusoidal-shaped filter for making the continuous interference happen: first, $\Delta\lambda$ should be small to bring the peaks close enough in both time domain and frequency domain (or wavelength domain) so that different peaks could have time-domain overlapping for interference, and will not be stopped by the severe walking-off effect caused by large center wavelength differences between different peaks; second, T_{min} needs to be large for imposing less attenuation to the joints of different peaks in frequency domain (or wavelength domain), in order to let the joints, which is also where the time-domain interference happens, survive in the iterations.

4. Conclusions

Spectrum filters with Gaussian-shaped profile, super-Gaussian-shaped profile and sinusoidal-shaped profile are employed in the simulations to investigate the impact of spectrum filtering on the pulse evolutions in an ANDi fiber laser. The Gaussian-shaped filter can introduce an attenuation related to the pulse spectrum width, which limits the pulse energy and generates extra gain. When background noises are amplified by a strong extra gain, the DS break up. The super-Gaussian-shaped filter barely affects the DS if the pulse spectrum width is much narrower than the filter bandwidth. However, the sharp edges in the transmission profile of the super-Gaussian-shaped filter are able to induce fluctuations in the pulse envelope and trigger the generation of NLP. For the sinusoidal-shaped filter, due to the multiple peaks in the transmission curve, DS with different central wavelengths can be generated. Under some circumstances, a single pulse with multiple peaks can be generated instead of the DS and these peaks could interfere with each other, which finally makes the pulse evolve into NLP.

The simulation results also indicate that to achieve DS with higher single pulse energies in ANDi mode-locked fiber lasers, from the point of view of spectral filtering, spectrum filters with larger bandwidths are preferred: for the Gaussian-shaped filter, the extra gain induced by the filter could be decreased so that DS are not easy to break up; for the super-Gaussian-shaped filter, the fluctuations introduced by the sharp edges of the filter to pulse envelope could be alleviated, which makes it harder for DS turning into NLP; for the sinusoidal-shaped filter, not only the extra gain is weakened, but also the NLPs generated from the multiple peaks could be avoided, therefore dissipative soliton break up and NLP generation can both can be suppressed.

Optics EXPRESS

Acknowledgments

The authors acknowledge the software development group of 'SeeFiberLaser' for providing help on the simulations and fruitful discussions.

Disclosures

The authors declare no conflicts of interest.

References

1. F. M. Mitschke and L. F. Mollenauer, "Ultrashort Pulses from the Soliton Laser," Opt. Lett. **12**(6), 407–409 (1987).
2. K. Tamura, E. P. Ippen, H. A. Haus, and L. E. Nelson, "77-Fs Pulse Generation from a Stretched-Pulse Mode-Locked All-Fiber Ring Laser," Opt. Lett. **18**(13), 1080–1082 (1993).
3. F. O. Ilday, J. R. Buckley, W. G. Clark, and F. W. Wise, "Self-similar evolution of parabolic pulses in a laser," Phys. Rev. Lett. **92**(21), 213902 (2004).
4. A. Chong, J. Buckley, W. Renninger, and F. Wise, "All-normal-dispersion femtosecond fiber laser," Opt. Express **14**(21), 10095–10100 (2006).
5. W. Chang, A. Ankiewicz, J. M. Soto-Crespo, and N. Akhmediev, "Dissipative soliton resonances," Phys. Rev. A **78**(2), 023830 (2008).
6. A. I. Chernykh and S. K. Turitsyn, "Soliton and Collapse Regimes of Pulse Generation in Passively Mode-Locking Laser Systems," Opt. Lett. **20**(4), 398–400 (1995).
7. M. Horowitz, Y. Barad, and Y. Silberberg, "Noiselike pulses with a broadband spectrum generated from an erbium-doped fiber laser," Opt. Lett. **22**(11), 799–801 (1997).
8. V. J. Matsas, D. J. Richardson, T. P. Newson, and D. N. Payne, "Characterization of a self-starting, passively mode-locked fiber ring laser that exploits nonlinear polarization evolution," Opt. Lett. **18**(5), 358–360 (1993).
9. L. A. Gomes, L. Orsila, T. Jouhti, and O. G. Okhotnikov, "Picosecond SESAM-based ytterbium mode-locked fiber lasers," IEEE J. Sel. Top. Quantum Electron. **10**(1), 129–136 (2004).
10. D. J. Richardson, R. I. Laming, and D. N. Payne, "Pulse repetition-rates in a passive, self-starting, femtosecond soliton fibre laser," (1991).
11. M. Nakazawa, E. Yoshida, and Y. Kimura, "Generation of 98 fs optical pulses directly from an erbium-doped fibre ring laser at 1.57 μm," Electron. Lett. **29**(1), 63–65 (1993).
12. D. J. Li, D. Y. Tang, L. M. Zhao, and D. Y. Shen, "Mechanism of Dissipative-Soliton-Resonance Generation in Passively Mode-Locked All-Normal-Dispersion Fiber Lasers," J. Lightwave Technol. **33**(18), 3781–3787 (2015).
13. Y. Du and X. Shu, "Pulse dynamics in all-normal dispersion ultrafast fiber lasers," J. Opt. Soc. Am. B **34**(3), 553–558 (2017).
14. X. Zhang, F. Li, K. Nakkeeran, J. Yuan, Z. Kang, J. N. Kutz, and P. K. A. Wai, "Impact of spectral filtering on multipulsing instability in mode-locked fiber lasers," IEEE J. Sel. Top. Quantum Electron. **24**(3), 1–9 (2018).
15. M. Alsaleh, T. Uthayakumar, E. T. Felenou, P. T. Dinda, P. Grelu, and K. Porsezian, "Pulse breaking through spectral filtering in dispersion-managed fiber lasers," J. Opt. Soc. Am. B **35**(2), 276–283 (2018).
16. Z. Wen, B. Lu, X. Qi, C. Zhang, K. Wang, H. Chen, and J. Bai, "Effects of spectral filtering on pulse dynamics in a mode-locked fiber laser with a bandwidth tunable filter," J. Opt. Soc. Am. B **36**(4), 952–958 (2019).
17. R.-Q. Xu, J.-R. Tian, and Y.-R. Song, "Noise-like pulses with a 14.5 fs spike generated in an Yb-doped fiber nonlinear amplifier," Opt. Lett. **43**(8), 1910–1913 (2018).
18. X. N. Zhu, "Explicit Jones Transformation Matrix for a Tilted Birefringent Plate with Its Optic Axis Parallel to the Plate Surface," Appl. Opt. **33**(16), 3502–3506 (1994).
19. D. Y. Tang, S. Fleming, W. S. Man, H. Y. Tam, and M. S. Demokan, "Subsideband generation and modulational instability lasing in a fiber soliton laser," J. Opt. Soc. Am. B **18**(10), 1443–1450 (2001).
20. D. Y. Tang, L.-M. Zhao, B. Zhao, and A. Q. Liu, "Mechanism of multisoliton formation and soliton energy quantization in passively mode-locked fiber lasers," Phys. Rev. A **72**(4), 043816 (2005).
21. X. X. Jin, L. Li, J. L. Luo, Y. Q. Ge, Q. Zhang, and L. M. Zhao, "Numerical Study on Autocorrelation of Noise-Like Pulse in Fiber Lasers," Laser Optoelectron. Prog. **52**, 173–179 (2015).

120.244.224.97 (ts 2024-08-06 10:21 SGT)